Document downloaded from:

http://hdl.handle.net/10251/188194

This paper must be cited as:

Kumar, V.; Mukherjee, M.; Lloret, J.; Ren, Z.; Kumari, M. (2021). A Joint Filter and Spectrum Shifting Architecture for Low Complexity Flexible UFMC in 5G. IEEE Transactions on Wireless Communications. 20(10):6706-6714. https://doi.org/10.1109/TWC.2021.3076039

The final publication is available at

https://doi.org/10.1109/TWC.2021.3076039

Copyright Institute of Electrical and Electronics Engineers

Additional Information

© 2021 IEEE. Personal use of this material is permitted. Permissíon from IEEE must be obtained for all other uses, in any current or future media, including reprinting/republishing this material for advertisíng or promotional purposes, creating new collective works, for resale or redistribution to servers or lists, or reuse of any copyrighted component of this work in other works.

A Joint Filter and Spectrum Shifting Architecture for Low Complexity Flexible UFMC in 5G

Vikas Kumar, *Student Member, IEEE*, Mithun Mukherjee, *Senior Member, IEEE*, Jaime Lloret, *Senior Member, IEEE*, Zhenwen Ren *Member, IEEE*, and Mamta Kumari, *Student Member, IEEE*

***Abstract*—The hardware realization of Universal Filtered Multi Carrier (UFMC) architecture has attracted significant attention in fifth generation (5G) and beyond. In addition to the flexibility in fast Fourier transform (FFT)-length, a flexible prototype filter in combination with multiplicative complex spectrum shifting co-efficients is required for realizing flexible UFMC architecture. The existing architectures of UFMC transmitter commonly adopted fixed-size FFT-length, number of subbands, subband size, and filter-length. Moreover, the lack of flexible prototype filter and spectrum localization of filter co-efficients to individual subbands limits the flexible UFMC system design. In this paper, we propose VLSI architecture for a flexible length prototype filter that can generate spectrally shifted filter co-efficients to individual subbands in tune with the changing value of FFT-length, number of subbands, subband size, and filter-length. For 16-bit word size architecture, our proposed design produces filter co-efficients and spectrum shifting co-efficients upto length, 2^{15}. Thus, any desired combination of FFT-length, number of subbands, subband size and filter-length is selected to generate the filter co-efficients for the individual subbands. Moreover, complex multiplication and addition operations are reduced in proposed architecture, quantitatively, about 58.81% reduction in filtering unit is achieved over the state-of-the-art architecture. Finally, hardware implementation output and XILINX post route simulation result matches perfectly with MATLAB simulations.**

***Index Terms*—5G and beyond, hardware implementation, flexible architecture, UFMC transmitter architecture**

I. Introduction

The advancement towards 5G and beyond wireless communication systems heavily depends on the choice of waveform candidates [1]–[5]. Recently, 5G New Radio (5GNR) standalone specification that is expected to support several emerging applications relies on orthogonal frequency-division multiplexing (OFDM) and its several alternative waveforms [1], [6], [7]. Interestingly, universal filtered multicarrier (UFMC) [8]–[10] is being considered as a potential candidate for future wireless communications due to its simplicity and the robustness over other variants of OFDM. In practice, after applying the filtered operation to a group of subcarriers in a subband, the out-of-band (OOB) sidelobe level is minimized in UFMC systems. This further results in minimum inter-block interference. In several cases, with the presence of hybrid analog/digital beamformers, the UFMC modulation is being studied for multiple-input multiple-output (MIMO) wireless link at mmWave carrier frequencies [11], [12].

In recent years, several authors have proposed complexity reduction schemes for UFMC design in multicarrier systems. For example, Jafri et. al. [13] proposed a complexity reduction method for inverse discrete Fourier transform (IDFT), finite impulse response (FIR)-filter, and spectrum shifting blocks. The proposed architecture results in a significant amount of savings in computations for UFMC implementation. Interestingly, five times fewer multipliers are used in FIR filter architecture than conventional architecture. Besides, a highly efficient method is introduced to compute spectrum shifting co-efficients through a small-sized lookup table [13]. Moreover, UFMC implementation with fast Fourier transform (FFT) pruning method was suggested by Saad et. al. [14]. Around 50% reduction in UFMC transmitter and receiver complexity is observed without any performance degradation. In 2020, Guo et.al. [15] introduced a FIR and a poly-phase filter structure approach to reduce the complexity based on the lightweight inverse fast Fourier transform (IFFT) method. By adjusting the filter parameters such as side lobe attenuation level, filter length, the performance of the system is improved. In addition to the time-domain filtering, fast convolution (FC)-based waveform [16]–[20] in UFMC architecture is widely used in recent times. These FC-based UFMC architecture designs provide flexibility in subcarrier-spacing (or symbol duration) and bandwidth of each subcarrier over conventional poly-phase time-domain filtering-based methods [15], [21], [22]. Interestingly, the FC-based UFMC architecture has shown a significant improvement over subband filtering when the prototype filter-length is high (i.e., above 50) [23]. The independent selection of the number of subbands and the bandwidth as well as the center frequency of each subband is regarded as one step forward to meet the 5G new radio (5G-NR) specifications [17].

Although, a significant amount of work is suggested towards UFMC hardware implementation and complexity reduction [13]–[15], [21], [24], existing architectures of UFMC have a common drawback as follows. The FFT length (N), number of subbands (B), subband size (N_b) and filter length (L) are fixed in these architectures [13]–[15], [21], [24]. This is mainly due to fixed size of filter co-efficients and spectrum

V. Kumar is with the Bharat Sanchar Nigam Limited, Patna, Bihar, India, 800001, e-mail: vikas.kumar@bsnl.co.in

M. Mukherjee is with the School of Artificial Intelligence, Nanjing University of Information Science and Technology, Nanjing 210044, China (e-mail: m.mukherjee@ieee.org). Corresponding author: Mithun Mukherjee

J. Lloret is with the Instituto de Investigación para la Gestión Integrada de Zonas Costeras (IGIC), Universitat Politecnica de Valencia, 46022 Valencia, Spain and also with the the School of Computing and Digital Technologies, Staffordshire University, Stoke ST4 2DE, U.K. (e-mail: jlloret@dcom.upv.es).

Z. Ren is with the Department of National Defence Science and Technology, Southwest University of Science and Technology, Mianyang 621010, China, and also with the Department of Computer Science, Nanjing University of Science and Technology, Nanjing 210094, China (e-mail: rzw@njust.edu.cn).

M. Kumari is with the Department of Computer Science and Engineering, Ramchandra Chandravansi Institute of Technology, Bishrampur, Jharkhand, India, 822132, e-mail: mamtarvs@gmail.com

shifting co-efficients. By changing the value of N, B, N_b, and L, the architecture demands a new set of values for the filter co-efficients as well as spectrum shifting co-efficients. An arrangement to generate new sets of values for these co-efficients will make UFMC architecture *flexible* that can be easily used for the multi-service provisioning.

A. Motivation

Hardware realization of flexible filters has been widely studied in [25]–[28]. Note that the spectrum shifting of filter co-efficients to the center of the subband is one of the significant steps in hardware realization of the UFMC transmitter. The existing literature has adopted a common approach to store the complex spectrum shifting co-efficients, afterward, these co-efficients are multiplied with the filtered subband IDFT outputs to bring them to their respective subband centers. However, such an arrangement results in fixed-size N, B, N_b, and L leading to a fixed-size UFMC architecture. To explain, the number of subbands, the number of subcarriers in a subband, and the filter-length cannot be changed. Although a flexible FFT architecture has been presented in [29], the design of flexible architecture for UFMC is limited by the fixed-size of filter and spectrum shifting co-efficients. This motivates us to design a flexible length filter jointly with a spectrum shifting architecture for the flexible UFMC transmitter.

B. Our Contribution

The main contributions of this paper include:

- We aim to design a flexible architecture for joint prototype filter and spectrum shifting of cosine windows in UFMC transmitter. The proposed architecture, using Blackman window as prototype filter, has the flexibility to choose filter length upto $2^{(d-1)}$, where d is the data-length of the architecture[1]. Accordingly, the proposed architecture has the flexibility to generate spectrum shifting co-efficients of length upto $2^{(d-1)}$.
- The proposed architecture requires one *filtering* and *spectrum shifting* for both I- and Q-channel, instead of two parallel filtering units in the state-of-the-art architectures.
- Moreover, the proposed flexible *filtering* and *spectrum shifting* architecture can be accommodated with flexible FFT architecture to produce a flexible UFMC transmitter without any change in hardware resources. We prototype the proposed architecture on the commercially available Field-Programmable Gate Array (FPGA) device.

C. Organization and Notation

The rest of the paper is organized as follows. Section II presents the UFMC transmitter model. Section III describes a brief discussion on *CO*-ordinate *R*otation *DI*gital *C*omputer (CORDIC) algorithm. The subband spectrum shifting of filter co-efficients is detailed in Section IV. We propose the filter co-efficients generation and spectrum shifting architecture in Section V. The FPGA prototyping and experimental results are presented in Section VI. Finally, conclusions are drawn in Section VII.

[1]As an example, for a 16-bit data-length architecture, the filter length can take any value up to $2^{15} = 32768$.

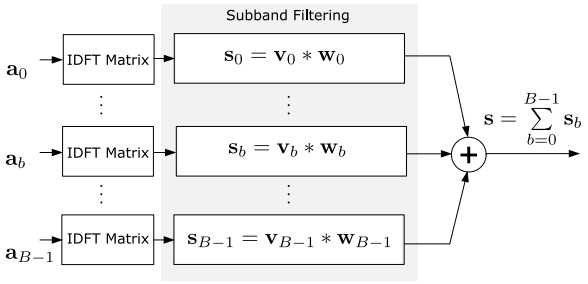

Fig. 1. System model of uplink baseband UFMC transmitter.

Notations used in the paper are as follows, bold lowercase letter (such as $\mathbf{a}$) denotes column vector, bold uppercase letters (such as $\mathbf{P}$) denote matrix, non-bold letters (such as w) denote scalar value. Linear convolution operation is denoted by $*$. Furthermore, c_0, c_1, and c_2 are multiplicative constants of generalized cosine window's (w), g_{in}^I and g_{in}^Q are in phase and quadrature component of a signal g_{in} (during filtering, g_{in} is selected as IDFT output sample points). G and γ denote magnitude and angle of the polar form of g_{in}, respectively.

II. UFMC Transmitter Model

As illustrated in Fig. 1, we consider an UFMC baseband transmitter with a total N number of subcarriers. These subcarriers are divided in B subbands. Denote N_b as the number of subcarriers in bth subband, thus, $BN_b \leq N$. We further denote $\mathbf{a}$ as N-dimensional input data symbols for the transmitter. Denote $\mathbf{a}_b$ as N-dimensional user data for the bth subband, and its subcarrier position-wise entry is expressed as

$$\mathbf{a}_b(u) = \begin{cases} \mathbf{a}(u) & \forall u \in \{bN_b,\, bN_b+1,\, \ldots\, (b+1)N_b-1\} \\ 0 & \text{otherwise} \end{cases} \tag{1}$$

for $u = 0, 1, \ldots, (N-1)$ and $b = 0, 1, \ldots, (B-1)$. Let $\mathbf{P}_b = \text{diag}\left([\mathbf{0}_{1\times N_b} \ldots \mathbf{1}_{1\times N_b} \ldots \mathbf{0}_{1\times N_b}]^T\right)$ be an N-dimensional matrix whose bth subband position has unit entry, thus, $\mathbf{a}_b = \mathbf{P}_b\mathbf{a}$. After performing an inverse Fourier transform (IFFT) over $\mathbf{a}_b$, we obtain $\mathbf{v}_b = \text{IFFT}(\mathbf{a}_b)$. Afterward, the vector $\mathbf{v}_b$ undergoes filtering stage by a L-dimensional finite impulse response (FIR) prototype filter $\mathbf{w} = [w_0, w_1, \ldots, w_{L-1}]$. Let $\mathbf{w}_b$ be the filter used for frequency localization of the vector $\mathbf{v}_b$ for the subband, b. The lth entry of the vector $\mathbf{w}_b = [w_{0,b}, w_{1,b}, \ldots, w_{L-1,b}]$ is defined as

$$w_{l,b} = w_l\, \exp(\phi_b), \quad l = 0, 1, \ldots, (L-1)\,, \tag{2}$$

where $\phi_b = 2\pi((N_b-1)/2 + b\,N_b)l/N$. Finally, the UFMC transmit signal is obtained as

$$\mathbf{s} = \sum_{b=0}^{B-1} \mathbf{s}_b = \sum_{b=0}^{B-1} \mathbf{v}_b * \mathbf{w}_b\,. \tag{3}$$

In the proposed architecture, it is a challenging issue *how to perform the spectrum shifting of window co-efficients* in (2). We use a well known CORDIC algorithm for the spectrum shifting, accordingly we present CORDIC algorithm before expounding the proposed work.

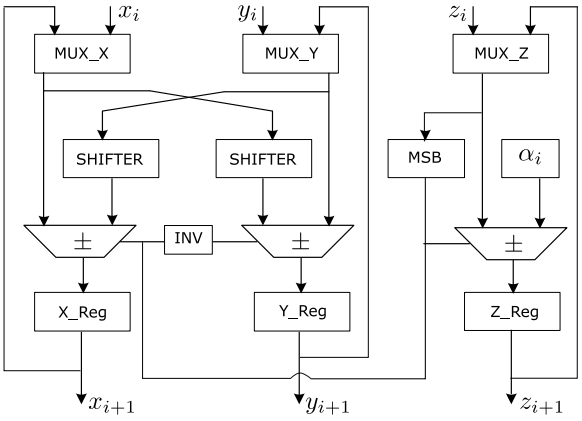

Fig. 2. Circular CORDIC architecture. MSB represents the sign bit of z_i, i.e., $\sigma_i = sign(z_i)$ and INV denotes an inverter block.

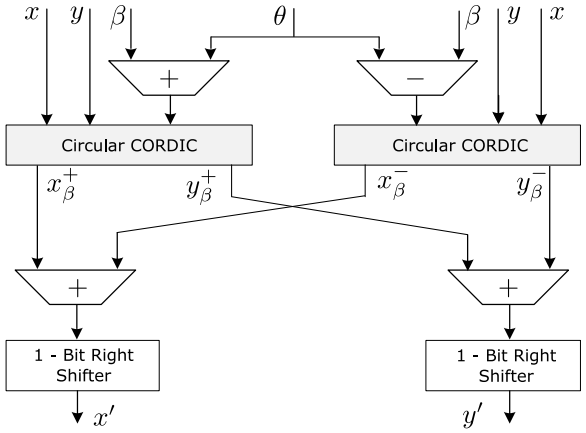

Fig. 3. Compensated CORDIC architecture.

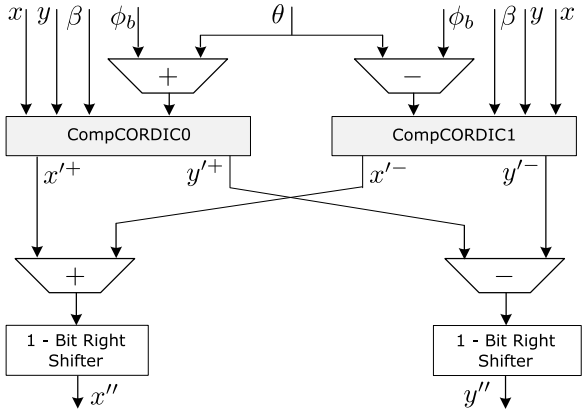

Fig. 4. Proposed spectrum shifting architecture for cosine term.

III. Background Work: Compensated CORDIC Architecture

CORDIC block with parallel compensation of scale factor is one of the main units in the proposed spectrum shifting approach. In the following, we discuss the parallel scale-factor compensation [30] in the CORDIC algorithm.

A. CORDIC Algorithm

In this work, we take circular CORDIC in a rotation mode. Denote $(x,\, y)$ as an initial vector that has to be rotated through an angle θ. The final vector denoted as $(x_{\rm f},\, y_{\rm f})$ can be represented in terms of initial vector as follows [28]:

$$\begin{aligned}\begin{bmatrix} x_{\rm f} \\ y_{\rm f} \end{bmatrix} &= \begin{bmatrix} \cos\theta & -\sin\theta \\ \sin\theta & \cos\theta \end{bmatrix} \begin{bmatrix} x \\ y \end{bmatrix} \\ &= \cos\theta \begin{bmatrix} 1 & -\tan\theta \\ \tan\theta & 1 \end{bmatrix} \begin{bmatrix} x \\ y \end{bmatrix} .\end{aligned} \tag{4}$$

As suggested by Volder [31], a set of iterative stages is performed to rotate the vector (x, y) in a step of predefined micro-rotation angles $\alpha_i = \tan^{-1}(2^{-i})$ such that θ can be accumulated in terms of α_i, i.e. $\theta = \sum_{i=0}^{m-1} \sigma_i \alpha_i$, where i varies from 0 to $(m-1)$, where m is an integer equal to the bit precision and $\sigma_i \in \{+1, -1\}$ depends on the rotation direction. Specifically, a hardware realization of the above CORDIC iteration stages, in case of each micro-rotation by dropping the $\cos\alpha_i$, can be expressed as

$$x_{i+1} = x_i - \sigma_i\, y_i\, 2^{-i}\,, \tag{5}$$

$$y_{i+1} = y_i + \sigma_i\, x_i\, 2^{-i}\,, \tag{6}$$

$$z_{i+1} = z_i - \sigma_i\, \alpha_i\,. \tag{7}$$

Note that the dropping of $\cos\alpha_i$ results an amplification in final rotated vector by a factor $K = 1/k$, where $k = \prod_{i=0}^{m-1} \cos\alpha_i$. Fig. 2 illustrates the circular CORDIC architecture, where the multiplexers MUX_X, MUX_Y, and MUX_Z select the input value of x, y and z, respectively. In addition, after every iteration, i, the registers X_Reg, Y_Reg, and Z_Reg store the output values of x, y, and z, respectively.

B. Parallel Scale-factor Compensation

To compensate the amplified CORDIC outputs, Villalba et. al. [30] suggested two CORDIC blocks in parallel, as illustrated in Fig. 3. They have introduced an angle, denoted as $\beta = \cos^{-1}(k)$. To rotate the vector (x, y) by an angle θ, the input angles to the two circular CORDIC blocks are initialized by $(\theta + \beta)$ and $(\theta - \beta)$ that result in output vectors from the CORDIC blocks as $(x_\beta^+,\, y_\beta^+)$ and $(x_\beta^-,\, y_\beta^-)$, respectively. Then, the final vector (x', y') is obtained as follows

$$\begin{aligned}x' &= \frac{x_\beta^+ + x_\beta^-}{2} = K(x\cos\theta\cos\beta - y\sin\theta\cos\beta) \\ &= K\cos\beta(x\cos\theta - y\sin\theta) = (x\cos\theta - y\sin\theta)\end{aligned} \tag{8}$$

and

$$\begin{aligned}y' &= \frac{y_\beta^+ + y_\beta^-}{2} = K(x\sin\theta\cos\beta + y\cos\theta\cos\beta) \\ &= K\cos\beta(x\sin\theta + y\cos\theta) = (x\sin\theta + y\cos\theta)\,.\end{aligned} \tag{9}$$

IV. Proposed Scheme for Spectrum Shifting of Window Co-efficients

Consider a generalized cosine window expressed as

$$w = c_0 + c_1\,\cos\theta_1 + c_2\,\cos\theta_2\,, \tag{10}$$

where c_0, c_1 and c_2 are constants having their values less than unity, $\{c_0, c_1, c_2\} < 1$, $\theta_1 = 2\pi\, l/L$, $\theta_2 = 4\pi\, l/L$, and $l = \{0, 1, \ldots, (L-1)\}$. Using (2), the window co-efficients for the bth subband are expressed as

$$w_b = w\, \exp(\phi_b) = c_0\, \exp(\phi_b) + c_1\, \cos\theta_1 \exp(\phi_b) + c_2\, \cos\theta_2\, \exp(\phi_b)\,. \tag{11}$$

From the above, we see that the spectrum shifting of window co-efficients, i.e., w_b is a summation of linear term c_0 and cosine terms $c_1 \cos\theta_1$, and $c_2 \cos\theta_2$ multiplied by $\exp(\phi_b)$. Basically, the term $c_0\, \exp(\phi_b) = c_0\, \cos\phi_b + j c_0\, \sin\phi_b$, can be realized by using (8) and (9) taking $x = 1$, $y = 0$, $\theta = \phi_b$, and $\beta = \beta_0 = \cos^{-1}(c_0 k)$. Therefore, the final vector can be expressed as

$$x'_0 = K \cos\beta_0 (x\cos\theta - y\sin\theta) = c_0 \cos\phi_b \tag{12a}$$
$$y'_0 = K \cos\beta_0 (x\sin\theta + y\cos\theta) = c_0 \sin\phi_b\,. \tag{12b}$$

As illustrated in Fig. 4, the computation for cosine term $c_1\, \cos\theta_1 \exp(\phi_b)$ can be realized using two parallel compensated CORDIC architecture, shown as CompCORDIC0 and CompCORDIC1. We take corresponding input angle $\theta = \theta_1 + \phi_b$ and $\theta_1 - \phi_b$ for the two compensated CORDIC blocks and $x = 1, y = 0$ and $\beta = \beta_1 = \cos^{-1}(c_1 k)$. So, the corresponding output vectors $(x'_1+,\, y'_1+)$ and $(x'_1-,\, y'_1-)$ of the CompCORDIC0 and CompCORDIC1 are expressed as

$$x'_1+ = c_1 \cos(\theta_1 + \phi_b)\,, \tag{13a}$$
$$y'_1+ = c_1 \sin(\theta_1 + \phi_b)\,, \tag{13b}$$
$$x'_1- = c_1 \cos(\theta_1 - \phi_b)\,, \tag{13c}$$
$$y'_1- = c_1 \sin(\theta_1 - \phi_b)\,. \tag{13d}$$

Afterward, the final output vector $(x''_1,\, y''_1)$ is obtained as

$$x''_1 = \frac{x'_1 + +x'_1-}{2} = \frac{c_1\cos(\theta_1+\phi_b) + c_1\cos(\theta_1-\phi_b)}{2} = c_1 \cos\theta_1 \cos\phi_b\,, \tag{14a}$$
$$y''_1 = \frac{y'_1 + -y'_1-}{2} = \frac{c_1\sin(\theta_1+\phi_b) - c_1\sin(\theta_1-\phi_b)}{2} = c_1 \cos\theta_1 \sin\phi_b\,. \tag{14b}$$

Similarly, $c_2 \cos\theta_1 \exp(\phi_b)$ can be realized by setting $x = 1$, $y = 0$, $\beta_2 = \cos^{-1}(c_2 k)$ and taking $\theta = \theta_2 + \phi_b$ and $\theta = \theta_2 - \phi_b$ for the two compensated CORDIC blocks, respectively in Fig. 4. Therefore, the output vectors become

$$x'_2+ = c_2 \cos(\theta_2 + \phi_b)\,, \tag{15a}$$
$$y'_2+ = c_2 \sin(\theta_2 + \phi_b)\,, \tag{15b}$$
$$x'_2- = c_2 \cos(\theta_2 - \phi_b)\,, \tag{15c}$$
$$y'_2- = c_2 \sin(\theta_2 - \phi_b)\,. \tag{15d}$$

Thereafter, we write the final output vector as

$$x''_2 = \frac{x'_2 + +x'_2-}{2} = \frac{c_2\cos(\theta_2+\phi_b) + c_2\cos(\theta_2-\phi_b)}{2} = c_2 \cos\theta_2 \cos\phi_b\,, \tag{16a}$$
$$y''_2 = \frac{y'_2 + -y'_2-}{2} = \frac{c_2\sin(\theta_2+\phi_b) - c_2\sin(\theta_2-\phi_b)}{2} = c_2 \cos\theta_2 \sin\phi_b\,. \tag{16b}$$

Now, from (12), (14), and (16), we obtain spectrum shifted window co-efficients for the bth subband as

$$x'_0 + x''_1 + x''_2 = (c_0 + c_1\cos\theta_1 + c_2\cos\theta_2)\cos\phi_b = w\cos\phi_b\,, \tag{17a}$$
$$y'_0 + y''_1 + y''_2 = (c_0 + c_1\cos\theta_1 + c_2\cos\theta_2)\sin\phi_b = w\sin\phi_b\,. \tag{17b}$$

Further by taking $x = g_{\text{in}}$ and $y = 0$ in (12), (14), and (16), we rewrite (17) as

$$x'_0 + x''_1 + x''_2 = g_{\text{in}}\, w\cos\phi_b\,, \tag{18a}$$
$$y'_0 + y''_1 + y''_2 = g_{\text{in}}\, w\sin\phi_b\,, \tag{18b}$$

where g_{in} can be selected as IDFT sample-points of a subband. In general, we need two such filters for both in-phase (I) and quadrature (Q) components of subband signal, assuming g_{in} in Cartesian form. This requirement of two filtering units for the I- and Q-channel can be reduced to a single filtering unit if g_{in} is available in polar form, i.e., $g_{\text{in}} = G\, \exp(\gamma)$, (Proof: see Appendix), by selecting $x = G$, $y = 0$, and replacing ϕ_b by $(\phi_b + \gamma)$ in (12), (14), and (16). Now, we rewrite (17) as

$$x'_0 + x'_1 + x'_2 = G\, w\cos(\phi_b + \gamma)\,, \tag{19a}$$
$$y'_0 + y'_1 + y'_2 = G\, w\sin(\phi_b + \gamma)\,. \tag{19b}$$

In the above discussion, we have used a 3-term cosine window. Note that for the windows having more than 3-term, (e.g., Blackman-Harris and Flat Top window), additional parallel compensated CORDIC blocks are needed. However, in the case of 2-term windows, such as Hamming window and Hann window, a smaller number of compensated CORDIC blocks is sufficient. Here, we propose an architecture for *filter* and *spectrum shifting* using the Blackman window. We express the Blackman window of length L as

$$w_{\text{bl}} = c_0 + c_1 \cos\frac{2\pi l}{L} + c_2 \cos\frac{4\pi l}{L}\,, \tag{20}$$

where $l = 0,\, 1\, \ldots\, (L-1)$, $c_0 = 0.42$, $c_1 = -0.5$, and $c_2 = 0.08$. Accordingly, we select $\beta_0 = \cos^{-1}(0.42\, k)$, $\beta_1 = \cos^{-1}(-0.5\, k)$, and $\beta_2 = \cos^{-1}(0.08\, k)$.

V. Proposed UFMC filtering and spectrum shifting architecture

Our proposed architecture generates the filter time samples as well as performs spectrum shifting of window co-efficients to bring them to their respective subband centers. Interestingly, this architecture simultaneously multiplies these shifted window co-efficients with IDFT sample points of the subband. Our proposed architecture is mainly based on (19) and (20). In Fig. 5, *EOC* stands for *end-of-computation* and shows the completion of each sample point computation. Besides, *Reset*, *Enable*, and *Clock* retain their usual meaning. The proposed architecture in Fig. 5 has three main blocks as below.

1) **Angle generator unit for window.** This unit generates angle sequences $\theta_1 = 2\pi l/L$ and $\theta_2 = 4\pi l/L$ according to the selected value of L. Later, these angle sequences

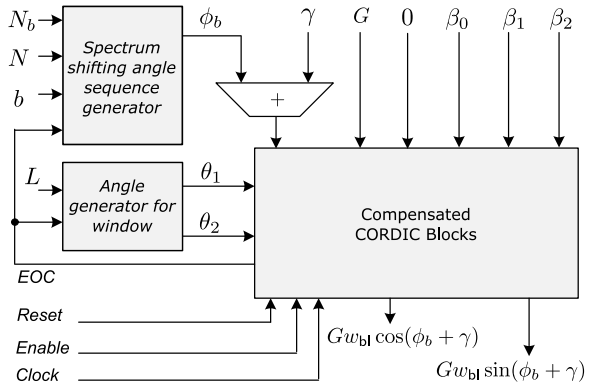

Fig. 5. Proposed UFMC filtering architecture.

are sent to the compensated CORDIC blocks. This angle generator unit has input as filter-length (i.e., L) and output as θ_1 and θ_2 as shown in Fig. 5. More details on the architecture mainly intended for the angle sequence generation are found in previous works [27], [28].

2) **Spectrum shifting angle sequence generator**. This unit generates angle sequence, i.e., ϕ_b for frequency domain shifting of filtered subband symbols to the center of the subband. It has input as IDFT-size (i.e., N), number of subcarriers in a subband (i.e., N_b), and subband index (i.e., b) for frequency domain shifting. Accordingly, the output generated by this unit becomes $\phi_b = 2\pi((N_b - 1)/2 + b\,N_b)\,l/N$, architecture for the angle sequence generation can be found in our previous work [32], [33].
3) **Compensated CORDIC blocks**. The proposed architecture uses five compensated CORDIC blocks, denoted as CompCORDIC $(00, 10, 11, 20, 21)$. As shown in Fig. 6, CompCORDIC00 computes $G\,c_0\,\exp(\phi_b+\gamma)$, while the pairs of compensated CORDIC blocks, i.e., {CompCORDIC10, and CompCORDIC11} and {CompCORDIC20, and CompCORDIC21} compute $G\,c_1\,\cos\theta_1\,\exp(\phi_b+\gamma)$ and $G\,c_2\,\cos\theta_2\,\exp(\phi_b+\gamma)$, respectively. Finally, we obtain the required output $G\,w_{\text{bl}}\,\cos(\phi_b+\gamma)$ and $G\,w_{\text{bl}}\,\sin(\phi_b+\gamma)$.

A. Computational complexity

Apart from the advantage of adding a unique flexibility to UFMC baseband transmitter, our proposed *filtering* and *spectrum shifting* architecture significantly reduces the required number of complex multiplication and addition operations in linear convolution of IDFT output samples with filter co-efficients and its spectrum shifting. We take the UFMC transmitter proposed by *Knopp et.al* [21] and examine the hardware and computational complexity reduction by integrating our proposed architecture. The comparative results are highlighted in Table I with the state-of-the-art architectures. We mainly analyse the complexity of the UFMC transmitter after the IDFT stage, i.e., filtering and spectrum shifting stage.

1) Classical UFMC [21]: Filtering is a linear convolution of the IDFT stage outputs and the filter co-efficients. We define the complexity of each subband as the number of complex multiplication and addition operations and express as $6NL + 2(N-1)(L-1)$ number of operations. So, overall complexity for total B subbands is given as

$$\mathcal{C}_{\text{class}} = B(6\,NL + 2(N-1)(L-1)) + 2(B-1)(N+L-1)\,. \tag{21}$$

Incorporating our proposed architecture in the classical UFMC filtering stage, complex operations per subband reduces to $NL + 2(N-1)(L-1)$ operations. Thus, overall complex operations using our proposed architecture be $B(NL+2(N-1)(L-1)) + 2(B-1)(N+L-1)$. As a result, an amount of $5BNL$ complex operations can be saved.

2) UFMC architecture proposed by Knopp et.al [21]: A complexity reduction scheme for UFMC architecture with N'-IDFT followed by upsampler with a upsampling factor $u = N/N'$ is proposed in [21]. The filtering operation is performed in two stages: a) first, by convolution of IDFT samples and filter co-efficients and b) later, spectrum shifting by multiplication of spectrum shifting co-efficients to bring the filtered IDFT output samples to their corresponding subband centers [21]. Basically, the convolution by filter co-efficients has a complexity of $2LN' + 2(N'-1)(L-u)$ and further spectrum shifting results in $6(N+L-1)$ number of complex operations of each subband. Therefore, an overall complex operation for filtering and spectrum shifting is expressed as

$$\mathcal{C}_{\text{knopp}} = B(2\,N'L + 2(N'-1)(L-u) + 6(N+L-1)) + 2(B-1)(N+L-1)\,. \tag{22}$$

3) Applying our proposed filter design in the architecture by Knopp et. al. [21]: In the following, we present the complexity saving in the linear convolution operation using the method by Knopp et. al. [21] in two different cases where IDFT stage outputs are available in both *Cartesian* and *Polar* form.

Case 1: *IDFT output in Cartesian form.* Here, two parallel filtering and spectrum shifting architecture of Fig. 5 are required for I- and Q-channel output of IDFT stage, i.e., keeping g_{in}^{Q} and g_{in}^{I} in place of G and $\gamma = 0$. The number of complex operations for each subband becomes $2N'L+2(N'-1)(L-u)$. Now, we write the overall complexity as

$$\mathcal{C}_{\text{proposed}}^{\text{rect}} = B\,(\,2N'L + 2(N'-1)(L-u)\,) + 2(B-1)(N+L-1)\,. \tag{23}$$

Thus, we can save a total $6B(N+L-1)$ amount of complex operation compared to [21].

Case 2: *IDFT output in Polar form.*[2] In this case, only one filtering and spectrum shifting architecture (illustrated in Fig. 5) is required for both I- and Q-channel. So, the number of complex operations for each subband can be expressed as $N'L + (N'-1)(L-u)$, and the overall complexity becomes

$$\mathcal{C}_{\text{proposed}}^{\text{polar}} = B\,(\,N'L + (N'-1)(L-u)\,) + 2(B-1)(N+L-1)\,. \tag{24}$$

As a result, total saving in complex operation compared to [21] can be expressed as $B\,(\,N'L+(N'-1)(L-u)+6(N+L-1)\,)$.

[2]Circular CORDIC in vectoring mode may be used for Cartesian to polar co-ordinate conversion [31].

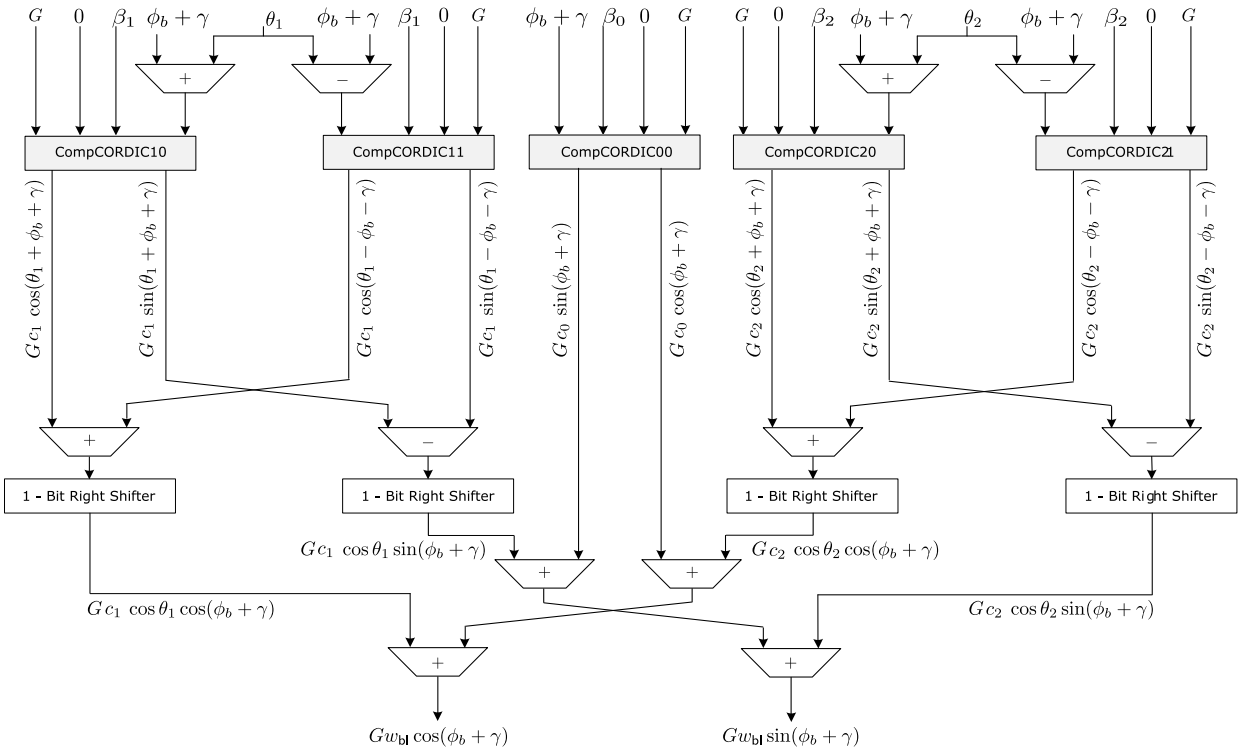

Fig. 6. Proposed architecture of compensated CORDIC blocks for prototype filter and spectrum shifting.

TABLE I
COMPARISON OF FILTERING AND SPECTRUM SHIFTING USED IN VARIOUS UFMC ARCHITECTURES

Architecture	**Saving in number of complex additions and complex multiplications operations**	**Flexibility**		**Co-efficient storage**	
		Filter	Spectrum shifting	Filter	Spectrum shifting
Classical UFMC [21]	$5\,BNL$	Fixed size	Fixed size	L	$2\,N$
Knopp et. al. [21]	$B(N'L+(N'-1)(L-u)+6(N+L-1))$	Fixed size	Fixed size	L	$2N$
Jafri et. al. [13]	$B(N'L+(N'-1)(L-u)+6\,(N+L-1))$	Fixed size	Fixed size	L	$\leq 2N$
Jafri et.al [22]	$B(N'L+(N'-1)(L-u)+6(N+L-1))$	Fixed size	Fixed size	L	$\leq (N+N/2)$
Guo et.al [15] linear-phase filter-based UFMC	$B(N'L+4\,(N+L-1))^{\dagger}$	Fixed size	Fixed size	$L/2$	$2\,N$
Guo et.al [15] poly-phase filter-based UFMC	$B\left(5\,N'\sum_{p=0}^{u-1}\left\lceil\frac{L-p}{u}\right\rceil+4(N+L-1)\right)^{\dagger}$	Fixed size	Fixed size	$L/2$	$2N$
Proposed		upto 2^{d-1}	upto 2^{d-1}	No storage	Not required

† Only complex multiplication operations are considered.

For example, similar to the system parameters in [21], we take $N = 1024$, $L = 72$, $N_b = 12$, and $N' = 64$. We observed a reduction of 62.50% and 58.81% in complex operations (without considering IDFT stage complexity) of the classical UFMC [9] and Knopp et.al. [21], respectively.

VI. SIMULATION RESULTS

We prototype a 16-bit word-size of the proposed architecture (illustrated in Fig. 5) on XILINX platform using Verilog hardware description language. For simulation, we have taken filter length, $L = 64$, IDFT size, $N = 256$, number of subbands, $B = 3$ and number of subcarriers in a subband, $N_b = 15$. The power spectral density (PSD) of the filter for continuous three subbands is shown in Fig. 7. From the figure, we observe that the Xilinx post route simulation outputs match closely with MATLAB simulations. Table II summarizes the device utilization report for the 16-bit word-size of proposed filtering and spectrum shifting architecture. Table III summarizes the figure-of-merit (FOM) parameters for MATLAB and XILINX post route simulation outputs for three different subbands. Further, Figs. 8 (a) and (b) show the PSD and time domain I- and Q-Channel, respectively, of the quadrature amplitude modulated (QAM) UFMC signal for the same three continuous subbands using the proposed filtering and spectrum shifting architecture. Fig. 8 (a) shows a comparison of the MATLAB simulation output and XILINX post route simulation data output. Similarly, we use Digilent Pmod-DA2 digital-to-analog converter (DAC), a 12-bit DAC powered by the Texas Instruments DAC121S101, for analog conversion of the baseband UFMC digital signal for both I- and Q-channel and shown in Fig. 8(b).

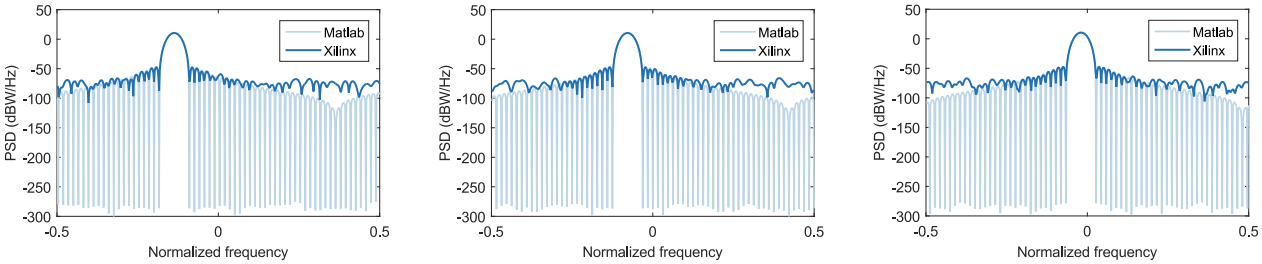

(a) Subband 1 (b) Subband 2 (c) Subband 3

Fig. 7. Three continuous subbands filters spectrum considering, prototype filter-Blackman, $L = 64$, IDFT size = 256, Number of subcarriers in a subband = 15 and setting initial subband offset = 85.

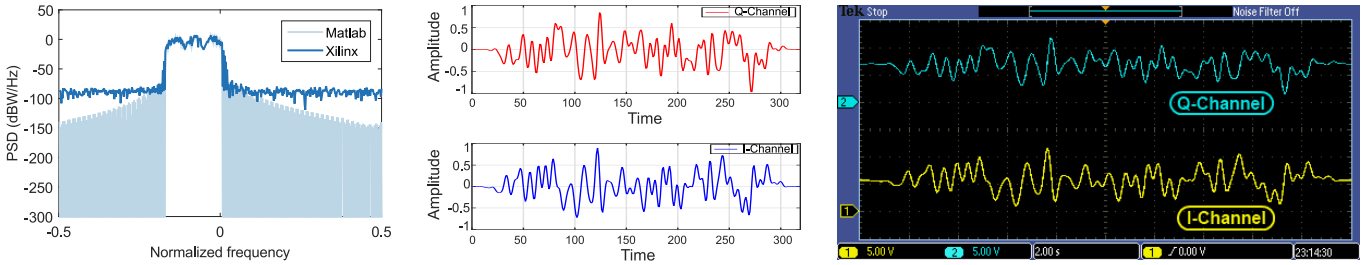

(a) (b) (c)

Fig. 8. Three continuous subbands of UFMC transmit signal (a) spectrum of UFMC MATLAB vs XILINX post route simulation output; (b) and (c) I- and Q-channel output of UFMC time domain signal of MATLAB and FPGA outputs. We take the prototype filter as Blackman, $L = 64$, IDFT size = 256, number of subcarriers in a subband = 15 and setting initial subband offset = 85.

TABLE II
DEVICE UTILIZATION SUMMARY (DEVICE - XC5VLX110T-1FF1136)

Units	Used	Available	% of Utilization
# Slice Registers	823	69120	1
# Slice look-up tables	2973	69120	4
# Flip-flop pairs	806	2990	26

A. Discussions and Future Direction

Critical path delay. In the proposed architecture, we use *folded* iterative CORDIC architecture [34], [35]. As a result, the maximum operating frequency, i.e., $f_{\max}$, is limited by critical path delay due to the adder (i.e., t_{adder}) as well as logical shifter (i.e., t_{shifter}). Therefore, we can write $f_{\max} = 1/(t_{\text{adder}} + t_{\text{shifter}})$.

Throughput. Note that throughput for the *folded* iterative CORDIC architecture is expressed as $f_{\max}/m$ [samples per second], where m is the number of iterative stages in the proposed CORDIC-based architecture. By using pipelined-CORDIC architecture, where wired shifting is used instead of logical shifter for each iteration, the maximum operating frequency, i.e, $f_{\max}$ is limited by t_{adder} only, i.e., $f_{\max} = 1/t_{\text{adder}}$ [samples per second]. Note that the throughput can be improved by using fast adders [36], [37].

Window selection. The proposed architecture for filtering and spectrum shifting in UFMC transmitter is limited to cosine windows only. The well-studied Dolph-Chebyshev window as well as recent optimized filters [38]–[40] are becoming attractive choice. These optimized filters consider the ratio among UFMC signal in-band distortion, and out-of-band radiation for different filter length and filter co-efficients. Our future work includes design and implementation of a flexible filtering and spectrum shifting architecture for these state-of-the-art windows. In the future, we aim to incorporate our proposed design in recently published work by Yi- Kaakinen et al. [17], [18], which is a very promising FC-based UFMC architecture to meet some of the requirements, such as flexible subcarrier-spacings/symbol-durations and spectrum localization of the subband in 5G-NR specifications. Our proposed architecture can be used to generate the subband frequency domain coefficients for FC-based filtering. We further plan to analyse and experiment the performance of UFMC system in presence of various channel models, multiple antenna application with externally controlled IFFT/FFT length [29], number of subbands, subcarriers within a subband, filter type and length.

VII. CONCLUSIONS

In this paper, we have proposed a hardware-efficient flexible filtering and spectrum shifting architecture in UFMC transmitter. The proposed architecture exhibits the flexibility to generate filter and spectrum shifting co-efficients for externally selected IDFT-size, number of subbands, number of subcarriers in a subband, and the pulse shaping filter-length without any changes in hardware resources. The experimental baseband signal corroborates the simulation results. Moreover, we have shown that the spectrally shifted filter co-efficients generated by proposed architecture match perfectly with the simulation results. The proposed flexible filtering and spectrum shifting architecture brings a unique flexibility in UFMC transmitter and is suitable for the 5G and beyond systems due to its flexibility, hardware efficiency, and reusing the several

TABLE III
COMPARISON POST ROUTE SIMULATION/MATLAB SIMULATION

FOM from PSD of prototype filter	Subband 1		Subband 2		Subband 3	
	MATLAB	XILINX	MATLAB	XILINX	MATLAB	XILINX
-3dB Bandwidth (kHz)	175.630	175.632	156.555	156.571	175.641	175.632
Highest side lobe level (in dBm)	-17.273	-17.715	-17.3722	-17.7128	-17.8313	-17.7128
Occupied band width (in kHz)	303.9	304.0	362.7	362.7	373.6	373.6

hardware components compared to the state-of-the-art. Data- and process-level pipelining can be used for further research to increase the throughput. As a part of future work, we aim to design flexible filtering and spectrum shifting architecture for an approximated cosine window near to Dolph-Chebyshev window with different filter length.

APPENDIX

Denote g_{in} as the IDFT stage output signal and can be expressed in Cartesian form as

$$g_{\text{in}} = g_{\text{in}}^{\text{Q}} + j g_{\text{in}}^{\text{I}} \,, \tag{25}$$

where g_{in}^{Q} and g_{in}^{I} are the Q- and I-component of g_{in}, respectively. Let $G = \sqrt{\left(g_{\text{in}}^{\text{Q}}\right)^2 + \left(g_{\text{in}}^{\text{I}}\right)^2}$. Then, after the multiplication of filter co-efficients (i.e., w) and spectrum shifting co-efficients (i.e., $\exp(j\phi_b)$) with IDFT output, we rewrite (18) as

$$\begin{aligned} g_{\text{in}}\, w\, e^{j\phi_b} &= w\, g_{\text{in}}^{\text{Q}} \exp(j\phi_b) + j\, w\, g_{\text{in}}^{\text{I}} \exp(j\phi_b) \\ &= w\, \left(g_{\text{in}}^{\text{Q}} \cos\phi_b - g_{\text{in}}^{\text{I}} \sin\phi_b\right) \\ &\quad + j\, w\, \left(g_{\text{in}}^{\text{Q}} \sin\phi_b + g_{\text{in}}^{\text{I}} \cos\phi_b\right) \\ &= G\, w \cos\left(\phi_b + \gamma\right) + j\, G\, w \sin\left(\phi_b + \gamma\right) \\ &= G\, w\, \exp(j(\phi_b + \gamma)) \,, \end{aligned} \tag{26}$$

where $\gamma = \tan^{-1}\left(g_{\text{in}}^{\text{I}} / g_{\text{in}}^{\text{Q}}\right)$. It is worthwhile to note that instead of using two parallel filter co-efficient and spectrum shifting co-efficient multiplication units for IDFT stage output signal g_{in}^{Q} and g_{in}^{I}, we use a single unit for $G\, w\, \exp\left(j(\phi_b + \gamma)\right)$.

REFERENCES

[1] X. Lin, J. Li, R. Baldemair, J. T. Cheng, S. Parkvall, D. C. Larsson, H. Koorapaty, M. Frenne, S. Falahati, A. Grovlen, and K. Werner, "5G new radio: Unveiling the essentials of the next generation wireless access technology," *IEEE Commun. Standards Mag.*, vol. 3, no. 3, pp. 30–37, Sept. 2019.

[2] T.-T. Lin and T.-C. Chen, "Complexity-reduced receiver for universal filtered multicarrier systems," *IEEE Wireless Commun. Lett.*, vol. 8, no. 6, pp. 1667–1670, Dec. 2019.

[3] X. Chen, L. Wu, Z. Zhang, J. Dang, and J. Wang, "Adaptive modulation and filter configuration in universal filtered multi-carrier systems," *IEEE Trans. Wireless Commun.*, vol. 17, no. 3, Mar. 2018.

[4] L. Zhang, A. Ijaz, P. Xiao, A. Quddus, and R. Tafazolli, "Subband filtered multi-carrier systems for multi-service wireless communications," *IEEE Trans. Wireless Commun.*, vol. 16, no. 3, pp. 1893–1907, Jan. 2017.

[5] D. Qu, F. Wang, Y. Wang, T. Jiang, and B. Farhang-Boroujeny, "Improving spectral efficiency of FBMC-OQAM through virtual symbols," *IEEE Trans. Wireless Commun.*, vol. 16, no. 7, pp. 4204–4215, Apr. 2017.

[6] S. Buzzi, A. Ugolini, A. Zappone, and G. Colavolpe, *An Introduction to Modulations and Waveforms for 5G Networks*. John Wiley & Sons Ltd., 2016, ch. 1, pp. 1–23.

[7] R. Zayani, Y. Medjahdi, H. Shaiek, and D. Roviras, "WOLA-OFDM: A potential candidate for asynchronous 5G," in *Prof. IEEE Globecom Wkshps*, Dec. 2016.

[8] V. Vakilian, T. Wild, F. Schaich, S. ten Brink, and J. Frigon, "Universal-filtered multi-carrier technique for wireless systems beyond LTE," in *Proc. IEEE Globecom Workshops (GC Wkshps)*, Dec. 2013, pp. 223–228.

[9] F. Schaich, T. Wild, and Y. Chen, "Waveform contenders for 5G - suitability for short packet and low latency transmissions," in *Proc. IEEE 79th Veh. Technol. Conf. (VTC Spring)*, May 2014, pp. 1–5.

[10] T. Wild and F. Schaich, "A reduced complexity transmitter for UF-OFDM," in *Proc. IEEE 81st Veh. Technol. Conf. (VTC Spring)*, May 2015, pp. 1–6.

[11] S. Buzzi, C. D'Andrea, D. Li, and S. Feng, "MIMO-UFMC transceiver schemes for millimeter-wave wireless communications," *IEEE Trans. Commun.*, vol. 67, no. 5, pp. 3323–3336, May 2019.

[12] H. N. Parajuli, J. Poëtte, and E. Udvary, "UF-OFDM based radio over fiber for 5G millimeter wave small cell radio access network," in *Proc. 11th Int. Symp. on Commun. Syst., Netw. Digit. Signal Process. (CSNDSP)*, July 2018, pp. 1–4.

[13] A. R. Jafri, J. Majid, M. A. Shami, M. A. Imran, and M. Najam-Ul-Islam, "Hardware complexity reduction in universal filtered multicarrier transmitter implementation," *IEEE Access*, vol. 5, pp. 13 401–13 408, July 2017.

[14] M. Saad, M. Alawieh, A. C. A. Ghouwayel, H. Hijazi, and S.-M. Omar, "On the hardware implementation of a reduced complexity UFMC chain," in *Proc. IEEE Int. Conf. Comput. and Appl. (ICCA)*, Aug. 2018.

[15] Z. Guo, Q. Liu, W. Zhang, and S. Wang, "Low complexity implementation of universal filtered multi-carrier transmitter," *IEEE Access*, vol. 8, pp. 24 799–24 807, Jan. 2020.

[16] J. Yli-Kaakinen and M. Renfors, "Optimized reconfigurable fast convolution-based transmultiplexers for flexible radio access," *IEEE Trans. Circuits Syst. II, Express Briefs*, vol. 65, no. 1, pp. 130–134, Apr. 2018.

[17] J. Yli-Kaakinen, T. Levanen, A. Palin, M. Renfors, and M. Valkama, "Generalized fast-convolution-based filtered-OFDM: Techniques and application to 5G new radio," *IEEE Trans. Signal Process.*, vol. 68, pp. 1213–1228, Feb. 2020.

[18] J. Yli-Kaakinen, T. Levanen, S. Valkonen, K. Pajukoski, J. Pirskanen, M. Renfors, and M. Valkama, "Efficient fast-convolution-based waveform processing for 5G physical layer," *IEEE J. Sel. Areas Commun.*, vol. 35, no. 6, pp. 1309–1326, Mar. 2017.

[19] J. Yli-Kaakinen, T. Levanen, M. Renfors, and M. Valkama, "Optimized fast convolution based filtered-OFDM processing for 5G," in *Proc. European Conf. on Networks and Communications (EuCNC)*, June 2017, pp. 1–6.

[20] J. Yli-Kaakinen and M. Renfors, "Flexible fast-convolution implementation of single- carrier waveform processing for 5G," in *Proc. IEEE Int. Conf. on Communication Workshop (ICCW)*, June 2015, pp. 1269–1274.

[21] R. Knopp, F. Kaltenberger, C. Vitiello, and M. Luise, "Universal filtered multicarrier for machine type communications in 5G," in *Proc. Eur. Conf. Netw. Commun. (EUCNC)*, June 2016, pp. 27–30.

[22] A. R. Jafri, J. Majid, L. Zhang, M. A. Imran, and M. N. ul Islam, "FPGA implementation of UFMC based baseband transmitter: Case study for LTE 10MHz channelization," *Wireless Commun. and Mobile Comput.*, vol. 2018, pp. 1–12, July 2018.

[23] M. Borgerding, "Turning overlap-save into a multiband mixing, downsampling filter bank," *IEEE Signal Process. Mag.*, vol. 23, no. 2, pp. 158–161, Mar. 2006.

[24] I. Baig, U. Farooq, N. U. Hasan, M. Zghaibeh, V. Jeoti, and M. Imran, "A low PAPR universal filtered multi-carrier system for 5G machine type communications," in *Proc. Wireless Days (WD)*, Apr. 2019, pp. 1–4.

[25] K. C. Ray and A. S. Dhar, "CORDIC-based unified VLSI architecture for implementing window functions for real time spectral analysis," *IEE Proc. Circuits, Devices and Syst.*, vol. 153, no. 6, pp. 539–544, Dec. 2006.

[26] K. C. Ray and A. S. Dhar, "ASIC architecture for implementing blackman windowing for real time spectral analysis," in *Proc. Int. Conf. Signal Process., Comm. Networking, ICSCN '07.*, Feb. 2007, pp. 388–391.

[27] K. C. Ray and A. S. Dhar, "CORDIC-Based VLSI Architecture for Implementing Kaiser-Bessel Window in Real Time Spectral Analysis," *J Sign Process Syst*, vol. 74, pp. 235 – 244, Feb. 2014.

[28] V. Kumar, K. C. Ray, and P. Kumar, "CORDIC-based VLSI architecture for real time implementation of flat top window," *Microprocessors and Microsystems*, vol. 38, no. 8, Part B, pp. 1063 – 1071, Nov. 2014.

[29] X. Chen, Y. Lei, Z. Lu, and S. Chen, "A variable-size FFT hardware accelerator based on matrix transposition," *IEEE Trans. VLSI Syst.*, vol. 26, no. 10, pp. 1953–1966, Oct. 2018.

[30] J. Villalba, J. A. Hidalgo, E. L. Zapata, E. Antelo, and J. D. Bruguera, "CORDIC architectures with parallel compensation of the scale factor," in *Proc. The Int. Conf. on Application Specific Array Processors*, July 1995, pp. 258–269.

[31] J. E. Volder, "The CORDIC trigonometric computing technique," *IRE Trans. Electron. Comput.*, vol. EC-8, no. 3, pp. 330–334, Sept. 1959.

[32] V. Kumar, M. Mukherjee, and J. Lloret, "Reconfigurable architecture of UFMC transmitter for 5G and its FPGA prototype," *IEEE Syst. Journal*, pp. 1–11, July 2019.

[33] V. Kumar, M. Mukherjee, and J. Lloret, "A hardware-efficient and reconfigurable UFMC transmitter architecture with its FPGA prototype," *IEEE Embedded Syst. Lett.*, pp. 1–1, Dec. 2019.

[34] B. Lakshmi and A. Dhar, "VLSI architecture for parallel radix-4 CORDIC," *Microprocessors and Microsystems*, vol. 37, no. 1, pp. 79–86, Feb. 2013.

[35] B. Lakshmi and A. S. Dhar, "CORDIC architectures: A survey," *VLSI Design*, vol. 2010, p. 19, Mar. 2010.

[36] P. Bhattacharyya, B. Kundu, S. Ghosh, V. Kumar, and A. Dandapat, "Performance analysis of a low-power high-speed hybrid 1-bit full adder circuit," *IEEE Trans. Very Large Scale Integr. (VLSI) Syst.*, vol. 23, no. 10, pp. 2001–2008, Sept. 2015.

[37] Y. Safaei Mehrabani and M. Eshghi, "Noise and process variation tolerant, low-power, high-speed, and low-energy full adders in CNFET technology," *IEEE Trans. Very Large Scale Integr. (VLSI) Syst.*, vol. 24, no. 11, pp. 3268–3281, Apr. 2016.

[38] X. Wang, T. Wild, F. Schaich, and A. Fonseca dos Santos, "Universal filtered multi-carrier with leakage-based filter optimization," in *Eur. Wireless 2014; 20th Eur. Wireless Conf.*, May 2014, pp. 1–5.

[39] X. Wang, T. Wild, and F. Schaich, "Filter optimization for carrier-frequency- and timing-offset in universal filtered multi-carrier systems," in *Proc. IEEE VTC Spring*, May 2015, pp. 1–6.

[40] H. Wang, Z. Zhang, Y. Zhang, and G. Yu, "Enhanced inter-sub-band interference suppression for universal filtered multi-carrier transmission," in *Proc. IEEE WCNC*, Mar. 2017, pp. 1–6.

Vikas Kumar (S'10) received the B.E. degree in electronics and communication engineering from the Institution of Engineers, India, in 2003, the M.Tech. degree in VLSI and CAD from the Thapar University, Patiala, India, in 2008, and the Ph.D. degree in electrical engineering from the Indian Institute of Technology Patna, Patna, India, in 2017. Currently, he is working as SDE-in-Charge with Bharat Sanchar Nigam Limited, Patna, India. He has worked in the field of electronic switching (EWSD, OCB, and C-DOT exchanges) and networking. He is a recipient of the 2016 CSPA Best Paper Award. He has published more than 15 peer-reviewed papers in reputed journals and conferences. His major research interests include development of real-time communication systems, VLSI implementation for digital signal processing, FPGA-based system design, CORDIC-based VLSI architectures, and mobile edge computing.

Mithun Mukherjee (S'10-M'15-SM'20) received the Ph.D. degree in electrical engineering from the Indian Institute of Technology Patna, Patna, India, in 2015. Currently, he is a Professor with the School of Artificial Intelligence, Nanjing University of Information Science and Technology, Nanjing, China. Dr. Mukherjee was a recipient of the 2016 EAI WICON, the 2017 IEEE SigTelCom, the 2018 IEEE Systems Journal, and the 2018 IEEE ANTS Best Paper Award. He has been a guest editor for IEEE Internet of Things Journal and IEEE Transactions on Industrial Informatics. His research interests include wireless networks, mobile edge computing, and intelligent edge computing.

Jaime Lloret (M'07–SM'10) received his M.Sc. in physics in 1997, his M.Sc. in electronic engineering in 2003, and his Ph.D. in telecommunication engineering in 2006. He is an associate professor at Universitat Politecnica de Valencia, chair of the Research Institute IGIC, and the Head of the Active and Collaborative Techniques and Use of Technologic Resources in the Education (EITACURTE) Innovation Group. He is also the Chair of the Working Group of the Standard IEEE 1907.1. He has been the Internet Technical Committee Chair of the IEEE Communications Society and the Internet Society for the term 2013–2015. Since 2016, he has been the Spanish Researcher with highest h-index in the Telecommunications journal list according to the Clarivate Analytics Ranking.

Zhenwen Ren (Member, IEEE) received the B.Sc. and M.Sc. degrees in communication and information system from Southwest University of Science and Technology (SWUST), Mianyang, China, in 2011 and 2014, respectively. He is currently pursuing the Ph.D. degree in control science and engineering with the Nanjing University of Science and Technology (NJUST), Nanjing, China, from 2017. He is working with the school of National Defence Science and Technology, SWUST. He has published 20+ peer-reviewed papers. His research interests include wireless sensor networks, computer vision, machine learning, deep learning, and industrial software.

Mamta Kumari (Student Member, IEEE) received the B.Tech. degree in electronics and communication engineering from Ran Vijay Singh College of Engineering and Technology (RVSCET), Jamshedpur, India, in 2006. She received M. Tech. degree in 2014 in Electronics and Communication from Manav Bharti University, Himachal Pradesh, India. She is currently pursuing the Ph.D. degree in Electronics and Communication with the Madhyanchal Professional University, Bhopal, India. She is working as assistant professor in Department of Computer Science Engineering, Ramchandra Chandravansi Institute of Technology, Bishrampur, Jharkhand, India. Her major research interests are wireless sensor networks, VLSI architecture design, and FPGA prototyping.